TOPOLOGICAL CORRELATION OF BRAIN SIGNALS

Jian Yin[1]*, Yuan Wang*[2]

[1]Department of Biostatistics, Nanjing Medical University, China
[2]Department of Epidemiology and Biostatistics, University of South Carolina, U.S.A.

ABSTRACT

Electroencephalography (EEG) is an important neurophysiological modality for understanding brain functions and disorders. Topological data analysis (TDA) can decode patterns in EEG signals that are not captured by standard temporal and spectral features. Gradient filtration is a recently advanced TDA framework for extracting topological features in a signal treated as a two-dimensional curve and filtered with a straight line moving in an arbitrary direction. In this study, we propose a new correlation measure for EEG signals by correlating topological features across multiple directions. We compare its performance with standard correlation measures in simulation studies and application to EEG signals recorded in dogs with epilepsy.

***Index Terms*—** Topological Data Analysis, Topological Signal Processing, Persistent Homology, EEG.

1. INTRODUCTION

Topological signal processing is a recently developed approach for decoding multiscale features in signals via persistent homology (PH), a key algorithm in topological data analysis (TDA) [1, 2, 3]. It reveals changes of topological structures across different temporal and spectral scales of signals that may not be observable through the standard signal processing methods [4, 5, 6, 7, 8, 9, 10].

Current topological signal processing frameworks involve topological feature extraction from signals after a sliding window embedding [4, 5, 6], or direct topological feature extraction and inference on signals in the temporal domain [7, 8, 9, 10]. The former framework have been applied in diverse research areas, including but not limited to financial and functional brain imaging time series, [11, 12, 13]. The latter framework decodes multiscale features in a signal through the topological evolution of time segments corresponding to amplitude below a horizontal threshold. To relax the constraint on thresholding direction, the *gradient filtration* introduced by [14] treats a signal as a two-dimensional curve and captures the topological evolution of arcs to one side of a straight line moving in an arbitrary direction. It allows us to decode topological information in a signal in different directions.

On the other hand, correlation is important for studying the relationship between the dynamics of signals. Standard measures such as Pearson's correlation coefficient and cross correlation measure the linear association between signal dynamics. Motivated by the idea of cross correlation correlating among shifts in two signals, we develop a topological correlation by correlating persistence features across gradient filtrations in two signals and empirically show that combining persistence features like persistence landscapes (PLs) across gradient filtrations better captures underlying similarity in signals. The topological correlation is also applied to study functional connectivity electroencephalography (EEG) recorded in dogs with epilepsy in preictal and interictal phases.

2. METHODS

We set out to extract topological features from a signal $g : [0, T] \to \mathbb{R}$ smoothed with a weighted Fourier series $\hat{g}$, as in [8]. By imposing a horizontal threshold on its amplitude, the time segments corresponding to amplitude below the threshold emerge and merge in the sublevel set

$$K_\lambda^0 := \{t \in [0, T] | \hat{g}(t) \leq \lambda\}, \tag{1}$$

as the threshold moves upward. The process is called a *sublevel-set filtration* and can be summarized using features of persistent homology [7, 10]. The longer a time segment persists through the filtration, the more likely it pertains to feature of the signal, rather than noise. Sublevel-set filtration has found some strong applications to EEG studies of brain disorders [7, 8, 9, 10]. One limitation is the direction in which we can extract the topological signal features.

Gradient filtration, on the other hand, allows us to filter a signal with a threshold oriented in an arbitrary direction [14]. By treating the smoothed $\hat{g}$ as a two-dimensional curve $\gamma_g : [0, 1] \to \mathbb{R}^2$, the method quantifies the topological evolution of the arcs on one side of γ_g cut off by a straight line, as expressed by the sublevel set:

$$K_\lambda := \{((t, y) \in \gamma_g | y + \kappa t \leq \lambda\}, \tag{2}$$

where $y + \kappa t = \lambda$ with a fixed gradient $-\kappa \in \mathbb{R}$ and increasing intercept $\lambda \in \mathbb{R}$ is a straight line in $\mathbb{R}^2$ moving in the

Grant acknowledgment: This work is funded through the Big Data Health Science Center (BDHSC) Pilot Project Program at the University of South Carolina.

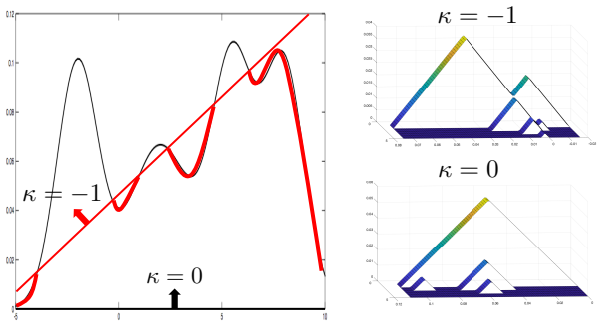

Fig. 1: Left: Gradient filtration with respect to two different directions ($\kappa = 0, -1$). The red arcs form a snapshot of the sublevel set in the gradient filtration with $\kappa = -1$. As the straight line moves in the direction of increasing λ (intercept of line), arcs emerge (birth) and merge (death) in the sublevel set. We code the corresponding λ as the birth and death times of the arcs in a barcode. Right: The persistence landscapes of the two filtrations constructed from the corresponding barcodes.

direction of increasing λ. Suppose the line touches the curve γ_g tangentially at $(t_{c_1}, g(t_{c_1})), \ldots, (t_{c_M}, g(t_{c_M}))$, i.e. y and t in the line $y + \kappa t = \lambda$ that satisfies

$$y - g(t_{c_i}) = g'(t_{c_i})(t - t_{c_i}), i = 1, \ldots, M,$$

as λ (intercept) of the line increases. The $t_{c_i}, i = 1, \ldots, M$, are critical points where the connectedness of the arcs in the sublevel set K_λ changes as the line moves in the direction of increasing λ (Figure 1 left). Assuming that the line hits at most one $g(t_{c_i})$ at a time, the process yields a sequence of sets of connected arcs $\emptyset = K_0 \subset K_1 \subset \cdots \subset K_M = \gamma_g$. In other words, if $\lambda_1 < \lambda_2 < \cdots < \lambda_M$ are the values of the intercept λ of the line as it hits the $t_{c_i}, i = 1, \ldots, M$ in γ_g, then $K_i = K_{\lambda_i}, i = 1, \ldots, M$, with $\lambda_0 = -\infty$. This process forms a *gradient filtration* on γ_g. At a merging junction, a younger arc dies and an elder arc survives (Elder Rule [2]).

To summarize the connectedness changes in the gradient filtration as birth and death of arcs occur, we use the topological feature *persistence landscape* (PL) [15]. We first encode the λ at which arcs emerge (birth) and merge (death) as endpoints of intervals collectively known as a *barcode*. Given an interval (a, b) in a barcode with $a \leq b$, we can define the piecewise linear bump function $h_{(a,b)} : \mathbb{R} \to \mathbb{R}$ by

$$h_{(a,b)}(\lambda) = \max(\min(\lambda - a, b - \lambda), 0). \tag{3}$$

The PL ν of $\{(a_i, b_i)\}_{i=1}^L$ is a multi-valued function defined as

$$\nu_l(\lambda) = \begin{cases} l\text{-th largest value of } \{h_{(a_i,b_i)}(\lambda)\}_{i=1}^L & 1 \leq l \leq L, \\ 0 & l > L. \end{cases} \tag{4}$$

Figure 1 (right) shows the PLs of gradient filtrations at two different gradients.

We now construct a new measure for **topological correlation** combining PLs of gradient filtrations across a range of gradients. The idea is to correlate areas under PLs constructed on these gradient filtrations. Consider two PLs v^1 and v^2 obtained from gradient filtration with respect to the gradient $-\kappa$ on two signals. We divide the nonzero base of PL $\{v^i\}$ equally into K parts:

$$x_1^i \leq \cdots \leq x_K^i,$$

where x_1^i and x_K^i are the minimum birth time and maximum death time of $\{v^i\}$. In each interval $(x_k^i, x_{k+1}^i), k = 1, \ldots, K-1$, A_{lk}^i represents the area under PL layer l of the i-th group from x_k^i to x_{k+1}^i . So the areas under all PLs of $\{v^i\}$ in the range of (x_k^i, x_{k+1}^i) are summed up as

$$A_{\cdot k}^i = \sum_{l=1}^{L} A_{lk}^i \tag{5}$$

where $k = 1, \cdots, K$. We obtain a series of $A_{\cdot k}^i$ and define the *topological correlation* between the two signals as the Pearson correlation between

$$(A_{\cdot 1}^1, \cdots, A_{\cdot K}^1) \text{ and } (A_{\cdot 1}^2, \cdots, A_{\cdot K}^2).$$

To enhance robustness of the topological correlation, we can combine different values $\kappa_1, \cdots, \kappa_J$ of κ. With different gradient $-\kappa_j$, we can get different PLs $\{v^{ij}\}$ and different set of $A_{\cdot n}^{ij}$. We calculate the average $A_{\cdot k}^{ij}$ as $\bar{A}_{\cdot k}^i$ under a series of $-\kappa_j$:

$$\bar{A}_{\cdot k}^i = \frac{\sum_{j=1}^J A_{\cdot k}^{ij}}{J} \tag{6}$$

where $k = 1, \cdots, K$. The topological correlation is then the Pearson correlation between

$$(\bar{A}_{\cdot 1}^1, \cdots, \bar{A}_{\cdot K}^1) \text{ and } (\bar{A}_{\cdot 1}^2, \cdots, \bar{A}_{\cdot K}^2).$$

3. SIMULATION STUDIES

We conduct two simulation studies to showcase the sensitivity of topological correlation in detecting the similarity between signals, in comparison with two standard correlation measures Pearson and cross correlation.

Study 1: Time shift. In this study, we test the sensitivity of topological correlation in detecting the similarity between signals after a shift in time, in comparison with the standard correlation measures. Consider a baseline signal:

$$y(t) = t\cos(\omega t)). \tag{7}$$

Using this baseline signal, we simulate four signals $y(t_i)$ at regular time intervals $0 \leq t_1, \cdots, t_{500} \leq 4\pi$:

$$y(t_i) = (t_i + d)cos(\omega(t_i + d)), \tag{8}$$

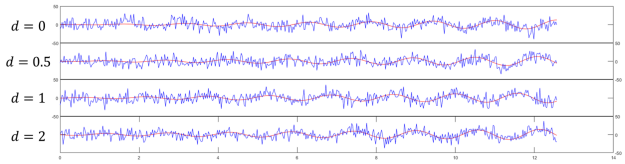

Fig. 2: Examples of the simulated signals in Study 1 when t' takes on the following values: 1) $t' = 0$; 2) $t' = 0.5$; 3) $t' = 1$; 4) $t' = 2$.

where $\omega = 4$ and d takes on four values: 1) $d = 0$ (no shift); 2) $d = 0.5$; 3) $d = 1$; 4) $d = 2$. When $d = 0$, it's just the baseline signal without any time shift. As d increases, the signal shifts in time. In each simulation, we add independent Gaussian noise at $0 \leq t_1, \cdots, t_{500} \leq 4\pi$:

$$y(t_i) = (t_i + d)cos(\omega(t_i + d)) + \epsilon_i, \tag{9}$$

where $\epsilon_i \sim N(0, 10^2)$. Examples of the simulated signals are shown in Figure 2. Then we calculate the topological correlation, Pearson correlation and cross correlation between the baseline signal and its time-shifted versions with noise and obtain their averages and standard deviations after 100 simulations. For better characterization of the topological structure of signals, we choose gradients in the range $0 \leq -\kappa_1, \cdots, -\kappa_{10} \leq 10$. PLs are constructed for each gradient $-\kappa_i$ and combined to compute the topological correlation.

Results in Table 1 show the means and standard deviations of the correlations under different time shifts. Topological correlation has the best performance in detecting signal similarity at the presence of time shift.

Study 2: Frequency scaling. In this study, we test the sensitivity of topological correlation in detecting the similarity between signals after frequency scaling. We follow the form of the four signals $y_1(t_i)$ as described in (8) and generate the following signals at regular time intervals $0 \leq t_1, \cdots, t_{500} \leq 4\pi$:

$$y_1(t_i) = (st_i)cos(\omega(st_i)), \tag{10}$$

where $\epsilon_i \sim N(0, 10^2)$ and s takes on four values: 1) $s = 1$ (no scaling); (2) $s = 0.5$; 3) $s = 2$; 4) $s = 5$. Examples

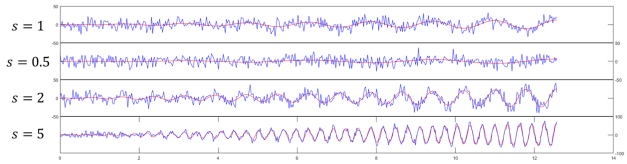

Fig. 3: Examples of the simulated signals in Study 2 when s takes on the following values: 1) $s = 1$; 2) $s = 0.5$; 3) $s = 2$; 4) $s = 5$.

Study 1	Time Shift Parameter d		
	0 vs 0.5	0 vs 1	0 vs 2
Topological Correlation	0.9489 (0.0175)	0.9711 (0.0158)	0.9512 (0.0184)
Cross Correlation	0.9330 (0.0037)	0.9252 (0.0040)	0.9393 (0.0035)
Pearson Correlation	-0.0860 (0.0447)	-0.1527 (0.0418)	-0.0266 (0.0496)
Normalized Mutual Information	0.8438 (0.0080)	0.8451 (0.0084)	0.8455 (0.0091)
Study 2	Frequency Scaling Parameter s		
	1 vs 0.5	1 vs 2	1 vs 5
Topological Correlation	0.9722 (0.0142)	0.9778 (0.0121)	0.9178 (0.0399)
Cross Correlation	0.9458 (0.0032)	0.9390 (0.0036)	0.9262 (0.0036)
Pearson Correlation	0.0020 (0.0399)	-0.0091 (0.0457)	0.0028 (0.0447)
Normalized Mutual Information	0.8450 (0.0084)	0.8468 (0.0086)	0.8523 (0.0077)

Table 1: Average topological, cross, and Pearson correlation and mutual information with corresponding standard deviation (in parentheses) in 100 simulated sets of signals.

of the simulated signals are shown in Figure 3. The gradient range is again set as $0 \leq -\kappa_1, \cdots, -\kappa_{10} \leq 10$ and PLs are combined over the $-\kappa_i$ to compute the topological correlation.

Results in Table 1 show that the topological correlation again performs better than the standard measures in detecting the underlying similarity in the signals at the presence of frequency scaling.

4. DATA APPLICATION

Epilepsy affects nearly 1% of the world's population, and is characterized by the occurrence of spontaneous seizures. Patients with epilepsy experience persistent anxiety due to the possibility of a seizure occurring. For 20-40% of patients with epilepsy, medications are not effective – and even after surgical removal of epilepsy-causing brain tissue, many patients continue to experience spontaneous seizures. Neurophysiological studies on animals provide insight into the disorder and improve treatment for human patients.

Data. The original datasets were collected and reported by [16]. Seven mixed-breed dogs with naturally occurring epilepsy and spontaneous seizures were housed in the University of Minnesota canine epilepsy monitoring unit. All dogs were implanted with the NeuroVista Seizure Advisory System and continuously monitored (24 hours/day) with video

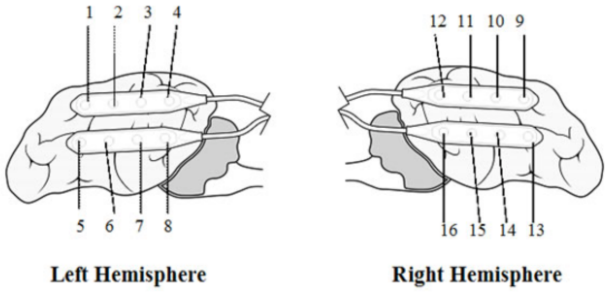

Fig. 4: The locations of 16 electrodes in the dogs' brains from which EEG signals are recorded. Figures are retrieved from the Kaggle competition forum.

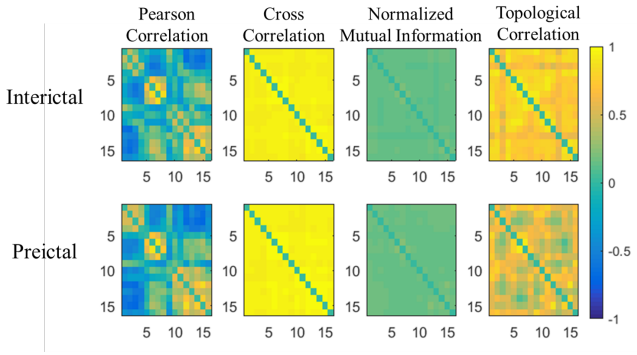

Fig. 6: Connectivity matrices in preictal and interictal phases.

and intracranial EEG. Only three had an adequate number of seizures and prolonged interictal recordings for data analysis. In this study, we chose data from dog 002 for analysis, as it showed the best seizure prediction accuracy (74%) out of seven dogs in [16], indicating relatively distinctive differences in the EEG signals of different seizure states. The EEG data sampled at 400 Hz from 16 electrodes (positions shown in Figure 4) with recorded voltages referenced to the 16 electrodes average was made accessible to the public from the Kaggle competition page: https://www.kaggle.com/c/seizure-prediction/data. Only interictal and preictal phases were provided in the dataset: the one-hour interictal phases was divided into six ten-minute segments, and the preictal phase covering one hour to five minutes prior to seizure onset was divided into six segments as well. The interictal and preictal EEG segments at 16 electrodes are shown in Figure 5.

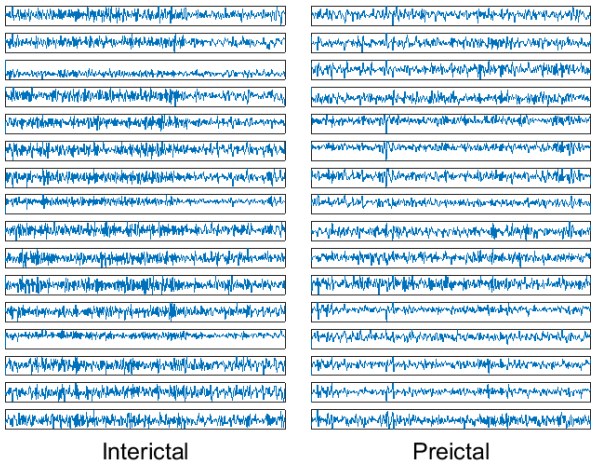

Fig. 5: An example of preictal and interictal EEG segments at 16 electrodes.

Results. The temporal dynamics of brain activity is classified into 4 states: interictal (between seizures, or baseline), preictal (prior to seizure), ictal (seizure), and post-ictal (after seizures). Here we use topological, Pearson, and cross correlation to analyze the preictal and interictal connectivity in the EEG signals across the 16 electrodes. Figure 6 shows connectivity matrices constructed from the three correlation measures between the signals of in preictal and interictal phases from 16 electrodes. We see that distinct difference between preictal and interictal connectivity constructed from topological correlation, while the connectivity constructed from Pearson and cross correlation is almost the same across the two phases. The p-values of ANOVA on different connectivity matrices in six preictal and interictal segments are shown in Table 2, where connectivity constructed from topological correlation does better overall in distinguishing the two phases better than that from the other measures.

Method	Segment					
	1	2	3	4	5	6
Topological	0.010	0.009	0.000	0.091	0.000	0.000
Cross	0.002	0.455	0.039	1.000	0.246	0.002
Pearson	1.000	1.000	1.000	1.000	1.000	1.000
NMI	0.972	0.000	0.040	0.066	0.274	0.807

Table 2: The p-values from ANOVA of topological, cross and Pearson correlation and normalized mutual information (NMI) in six preictal and interictal segments.

5. DISCUSSION

Correlation measures are important for studying relationship between signals recorded at different spatial locations, such as electrodes in EEG and brain regions of interest in magnetic resonance imaging. The proposed topological correlation measure decodes relationship between signals across multiple temporal and spectral scales. It may also be investigated in the context of periodicity.

6. REFERENCES

[1] H. Edelsbrunner, D. Letscher, and A. Zomorodian, "Topological persistence and simplification," *Discrete Computational Geometry*, pp. 511 – 533, 2002.

[2] H. Edelsbrunner and J.L. Harer, *Computational Topology*, American Mathematical Society, 2010.

[3] G. Carlsson, "Topology and data," *Bulletin of the American Mathematical Society*, vol. 46, pp. 255 – 308, 2009.

[4] J. Perea and J. Harer, "Sliding windows and persistence: An application of topological methods to signal analysis," *Foundations of Computational Mathematics*, vol. 5, pp. 799 – 838, 2015.

[5] J. Perea, "Persistent homology of toroidal sliding window embeddings," *Proceedings of the IEEE International Conference on Acoustics, Speech and Signal Processing (ICASSP)*, pp. 6435 – 6439, 2016.

[6] C. Tralie and J. Perea, "(quasi)periodicity quantification in video data, using topology," *SIAM Journal on Imaging Sciences*, vol. 11, pp. 1049 – 1077, 2018.

[7] Y. Wang, H. Ombao, and M.K. Chung, "Topological data analysis of single-trial electroencephalographic signals," *Annals of Applied Statistics*, vol. 12, pp. 1506–1534, 2018.

[8] Y. Wang, H. Ombao, and M.K. Chung, "Statistical persistent homology of brain signals," *Proceedings of the IEEE International Conference on Acoustics, Speech, and Signal Processing (ICASSP)*, pp. 1125 – 1129, 2019.

[9] Y. Wang, R. Behroozmand, L.P. Johnson, and J. Fridriksson, "Topology highlights neural deficits of post-stroke aphasia patients," *Proceedings of the IEEE International Symposium on Biomedical Imaging (ISBI)*, pp. 754 – 757, 2020.

[10] Y. Wang, R. Behroozmand, L.P. Johnson, L. Bonilha, and J. Fridriksson, "Topological signal processing and inference of event-related potential response," *Journal of Neuroscience Methods*, vol. 363, pp. 109324, 2021.

[11] M. Gidea and Y. Katz, "Topological data analysis of financial time series," *Physica A: Statistical Mechanics and its Applications*, vol. 491, pp. 820 – 834, 2018.

[12] S. Majumdar and A. Laha, "Clustering and classification of time series using topological data analysis with applications to finance," *Expert Systems with Applications*, p. 113868, 2020.

[13] T. Songdechakraiwut and M.K. Chung, "Dynamic topological data analysis for functional brain signals," *Workshop Proceedings of IEEE 17th International Symposium on Biomedical Imaging (ISBI)*, 2020.

[14] Y. Wang, R. Behroozmand, L.P. Johnson, L. Bonilha, and J. Fridriksson, "Topological signal processing in neuroimaging studies," *Proceedings of the IEEE International Symposium on Biomedical Imaging (ISBI)*, p. 10, 2020.

[15] P. Bubenik, "Statistical topological data analysis using persistence landscapes," *Journal of Machine Learning Research*, vol. 16, pp. 77 – 102, 2015.

[16] J. J. Howbert, E. E. Patterson, S. M. StEad, B. Brinkmann, V. Vasoli, D Crepeau, C. H. Vite, B. Sturges, V. Ruedebusch, and J. Mavoori, "Forecasting seizures in dogs with naturally occurring epilepsy," *Plos One*, vol. 9, 2014.